IOP Conf. Series: Materials Science and Engineering **179** (2017) 012059 doi:10.1088/1757-899X/179/1/012059

Evaluation of in-situ deformation experiments of TRIP steel

J Procházka, L Kučerová, M Bystrianský

RTI, UWB in Pilsen, Universitni 8, 30614 Pilsen, Czech Republic, EU

E-mail: jprochy@rti.zcu.cz, skal@rti.zcu.cz

Abstract: The paper reports on the behaviour of low alloyed TRIP (transformation induced plasticity) steel with Niobium during tensile test. The structures were analysed using in-situ tensile testing coupled with electron backscattering diffraction (EBSD) analysis carried out in scanning electron microscope (SEM). Steel specimens were of same chemical composition; however three different annealing temperatures, 800 °C, 850 °C and 950 °C, were applied to the material during the heat treatment. The treatment consisted of annealing for 20 minutes in the furnace; cooling in salt bath after the heating and holding at 425 °C for 20 minutes for all the samples. Untreated bar was used as reference material. Flat samples for deformation stage were cut out of the heat-treated bars. In situ documentation of microstructure and crystallography development were carried out during the deformation experiments. High deformation lead to significant degradation of EBSD signal.

1 Introduction

In-situ testing presents a new advanced method of material characterisation and testing. It can be performed in various kinds of microscopes to fit various purposes [1-4]. Scanning electron microscopes (SEM) provides suitable compromise between very high resolution but very small samples of transmission electron microscopy (TEM) and large observed area at low magnification of light microscopy. This is the reason why in-situ SEM testing is convenient for high strength steels analysis [3-5].

There are several grades of high strength steels with multiphase microstructures, whose mechanical properties depend strongly on volume fraction and morphology of individual phases and structural components. At least three grades of advanced high strength steels rely on carefully controlled amount of metastable retained austenite in the final microstructure [6-9]. To understand the behaviour of these steels under straining, it is important to establish how the phases react to external loading. Retained austenite in these steels tend to transform to martensite at room temperature during plastic deformation. The stability of retained austenite against this deformation induced transformation depend on the size, morphology and carbon content of each austenitic island, which makes the behaviour of these steels quite tricky to describe [10].

There are several challenges connected with preparation of large areas for electron backscattering diffraction (EBSD) analysis and testing of small samples. Deformation of ductile samples is not homogeneously distributed along the axe of the sample, the highest being local deformation around fracture area. To establish local deformation in the area observed during the test, measuring methodology has to be set up. Various sample shapes and geometries can be used for a particular deformation stage. Depending on the aim of the experiment, it might be practical to use either simple dog-bone shaped sample or some variations with more complicated geometry of the central part.

It should be also noted that every stage requires a minimal length of the sample, which is necessary to enable sample mounting into the stage.

2 Experimental details

2.1 Materials description

Low alloyed high strength TRIP (transformation induced plasticity) steel was used for this work. The steel had 0.2 % C and was further alloyed by 1.5 % Mn, 2 % Si and micro-alloyed by 0.06 % Nb. Manganese is typically added to TRIP steels to support retained austenite stabilization. Silicon is also very frequently found in TRIP steels as it increase the strength of the steel by solid solution strengthening and hinders cementite formation during the processing of the steel. The less carbides are formed the higher carbon content is available to diffuse into remaining austenite and thus increase its stability against martensitic transformation during final cooling of the steel. The original microstructure of the steel after casting, re-forging into the bars and annealing was ferritic-pearlitic.

The steel was further heat treated in the furnace by intercritical annealing at three temperatures of 800 °C, 850 °C and 900 °C for 20 minutes. All the samples were subsequently cooled to the temperature of 425 °C in a salt bath and 20 minutes long bainitic hold at this temperature took place in the second furnace. Resulting microstructures in all the samples consisted of the mixture of free ferrite, bainite, retained austenite and eventually M-A constituent (Figure 1). Around 10 % of retained austenite was found in the final microstructures by X-ray diffraction phase analysis.

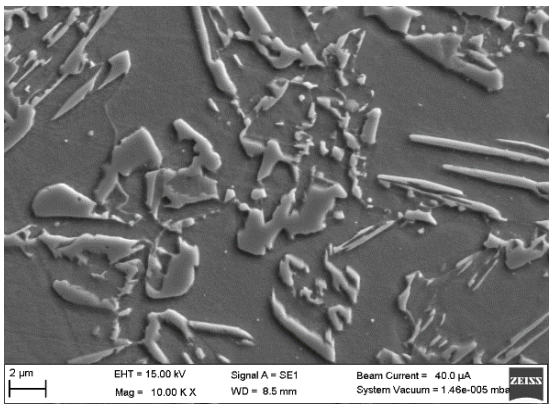

Figure 1. Multiphase TRIP microstructure, 800 °C annealing temperature.

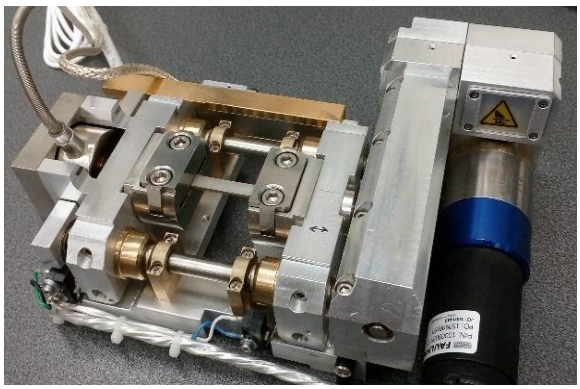

Figure 2. Deformation stage.

2.2 Tensile testing

Deformation stage MTII/Fullam (Figure 2) placed in the SEM Zeiss EVO 25 equipped with energy dispesion X-ray spectrometer (EDX) and EBSD detectors (both from Oxford Analytical) was used for the experiment. This stage is designed for testing inside the SEM chamber with loading force up to 10 kN. Tensile tests described in this work were carried out at room temperature, however the stage enables heating of the samples up to 1200 °C during loading experiments. The stage was tilted 70 °towards EBSD detector during some of the measurement. When only SEM images of etched microstructure were taken, the samples were perpendicular to the electron beam.

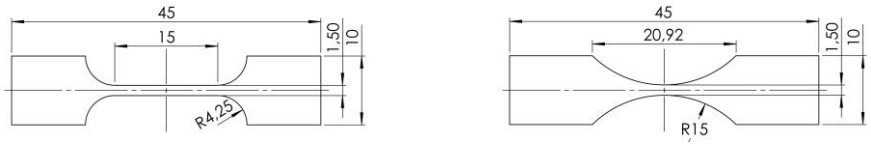

Figure 3. Sample geometries used for in-situ tensile tests: plain (left) and curved (right).

The samples were cut using water jet in slices and then to the final shapes. The samples were customized to fit in the deformation stage. Two geometries were used, one for load-strain measurement and tensile strength evaluation, further indicated as 'plain' and the second one had a neck in the central part aimed to observe the fracture initiation mechanism, further indicated as 'curved' (Figure 3).
Prior the SEM analyses tensile tests were carried out to obtain mechanical properties using as-delivered plain samples. Elongation rate was kept $\dot{l} = 1$ mm/min. Prior to the in situ analyses, the samples were ground and polished using 1µm diamond paste. Samples dedicated to SEM analysis were etched in 3% Nital, while samples intended for EBSD analysis were electrolytically polished to obtain deformation-free surface.

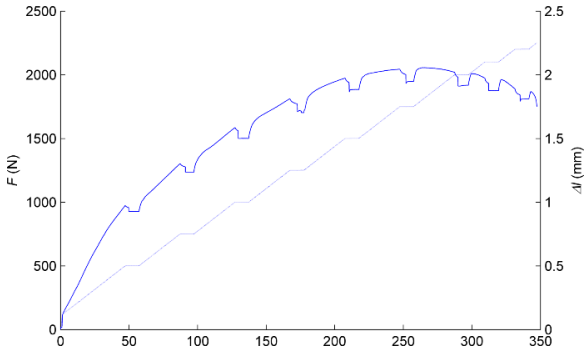

Figure 4. Time evolution of Load L and elongation Δl during tensile test with EBSD.

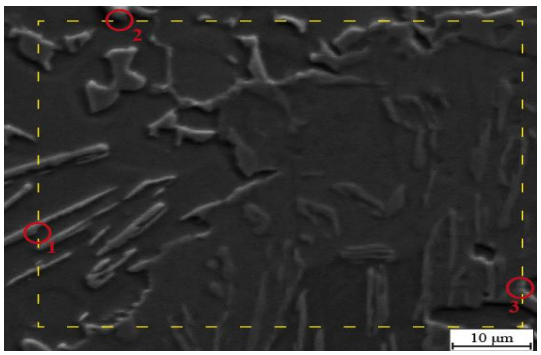

Figure 5. Emphasized points used for estimation of the strain induced in material.

The EBSD maps were obtained using tensile stage tilted to 70 ° and the tensile tests were interrupted several times to acquire desired data. The time evolutions of loading force F and elongation Δl are shown in Figure 4. During in-situ analyses the strain rate was set to lower value of $\dot{l} = 0.5$ mm/min. During the test several pauses had to be made to capture SEM images and perform EBSD measurements. In case of curved samples tests were paused at given elongations: $\Delta l = 0.5, 1.0, 1.25, 1.5, 1.75$ and 2.0 mm. In case of flat samples pauses were made at elongations $\Delta l = 0.5 - 4.0$ mm with step of 0.5 mm. In both cases when the ultimate strength of the specimen was reached, the tests were paused manually to observe the deformations and crack formation and propagation. The notches in the loading curves are caused by pausing the deflection therefore the stresses induced during deformation can relax. To prevent data log overflow, the planned pauses were set to 10 seconds each. Within this period, the sampling was paused manually allowing enough time (10-20 minutes) for EBSD maps and SEM images to be acquired. These manual pauses caused the sharp drops in the measured load in the scheduled pause period.
Stress-strain curves were evaluated from acquired data for plain samples using engineering stress $\sigma_e = \frac{F}{A_0}$ and strain $\varepsilon = \frac{\Delta l}{l_0}$, where A_0 and l_0 were calculated from sample dimensions, see Figure 3. Because of the shape of the curved sample the stress-strain curves could not be evaluated, unprocessed load-deflection curves are presented instead. The strain achieved in observed areas at each stop was estimated from position of three points chosen in every observed area (Figure 5).

3 Results

3.1 Effect of thermal processing on tensile strength

TRIP steel with niobium used in this work can possess very good combination of high ultimate tensile strength and excellent ductility after various heat or thermo-mechanical treatments. In the case of this work, tensile strength of three samples after heat treatments showed the strengths around 800 MPa with ductility approaching 40 % (Figure 6). Mechanical properties of the same steel in the original state before heat treatment are also shown in the graph by dark blue curve. It is apparent that original ferritic-

pearlitic microstructure had lower strength and distinctively shorter area of homogeneous plastic deformation. The comparison of the curves support general explanation, that gradual transformation of retained austenite to martensite during plastic deformation postpones the onset of necking of the steel.

Once the continuous tensile test was performed, the stops for discontinuous testing were planed (Figure 7) and the tests were carried out. Each drop on the force – elongation curve corresponds to one pause in the test, during which either microstructure observation or EBSD analysis were performed.

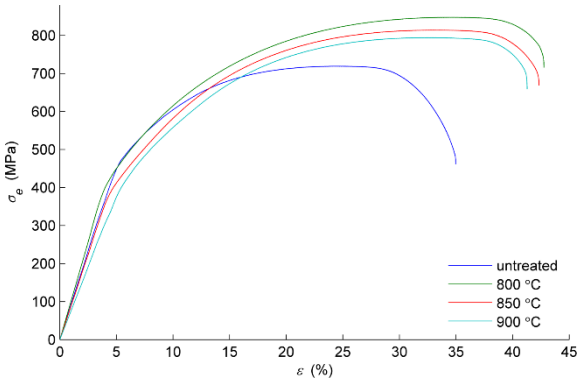

Figure 6. Engineering stress versus engineering strain.

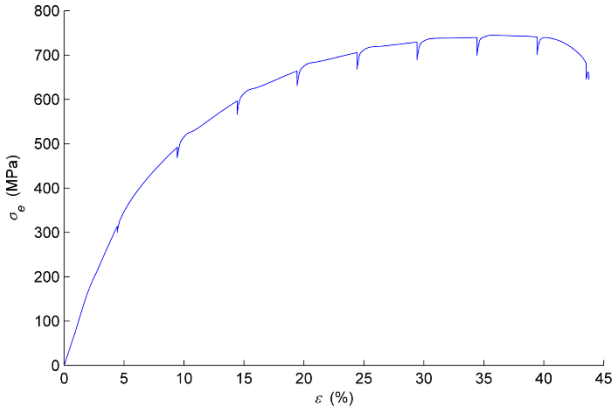

Figure 7. Stress-strain curve for EBSD experiment of the plain sample annealed at 900 °C.

3.2 Structure evolution prior to material failure

Microstructure development was observed during the pauses of tensile straining of the steel treated with 800 °C heating temperature. Representative stops were chosen and obtained microstructure images are shown in the Table 1. The images make it clear that cracks initiated at the highest load of 2 226 N, which corresponds to the ultimate strength of the steel. Fracture originated in this case from the free surface of the sample and the second crack just under the surfaces. Both of the origins used the presence of small hard grains in the microstructure and the cracks propagated along free ferrite – bainite interphase. Curved sample shape was used for this particular experiment to help to identify the most probable fracture initiation area.

The composite images in Figure 8 show the movement of individual phases and structural component during the test, for the sample heated to 900 °C (left) and 800 °C (right). It indicates that close to parallel bainitic laths are moving significantly less than individual smaller bulky items of the microstructure.

Table 1. Fracture initiation and crack propagation during final stages of the tensile test.

Δl [mm] *F* [N] ε [%]	Microstructure and fracture initiation	Δl [mm] *F* [N] ε [%]	Microstructure and fraction propagation
1.25 1 814 6.7	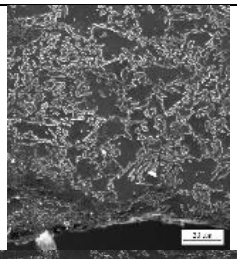	2.30 2 167 39.8	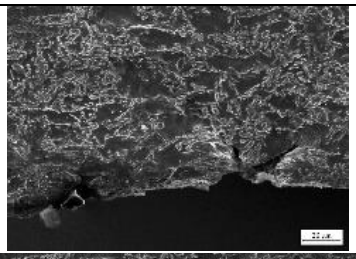
2.10 2 226 28.3	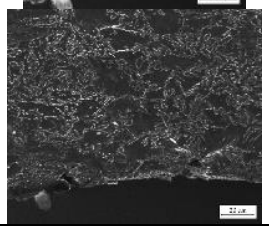	2.48 2 003 51.4	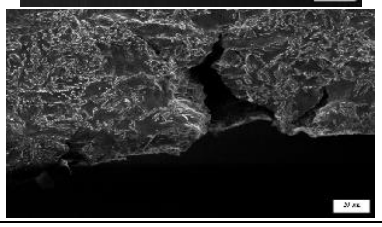

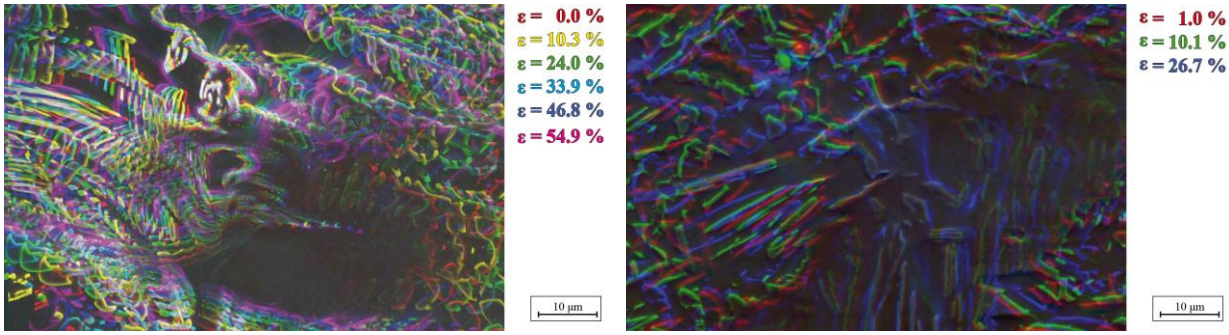

Figure 8. Composite figure of sample surface with various strain. The stress is applied in horizontal direction. Sample with 850 °C heating temperature (left) and 800 °C heating temperature (right).

The deformation occurs mainly in soft ferritic grains; harder areas of retained austenite or M-A constituent are dragged by the material flow. Small grains keep their shape and change only their position and orientation. Indicated deformation values were calculated from the gradual shifts of three chosen points during the straining (Figure 5).

Table 2. Band contrast, inverse pole figure and phase map derived from EBSD analysis of the microstructure development during tensile test of sample heated at 850 °C.

ε [%]	σ_e[MPa]	Band contrast	IPF-Z	Phase map
0	0	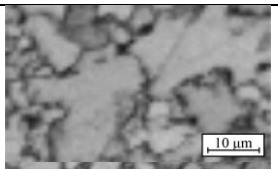		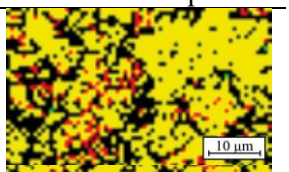
4.4	314	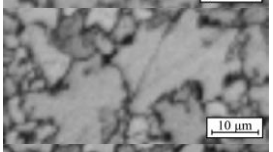		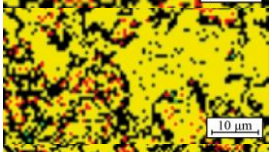
9.3	492		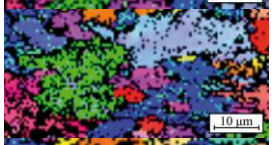	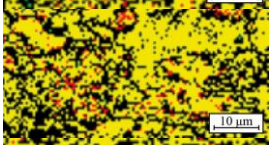
14.4	597	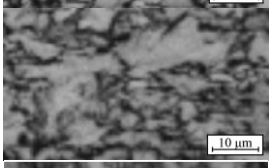		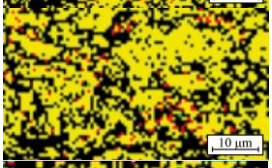
19.3	664	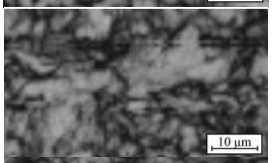	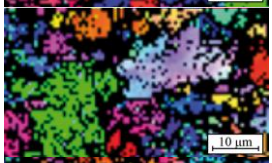	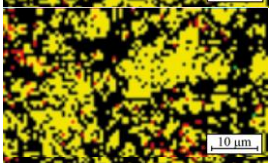
29.3	729	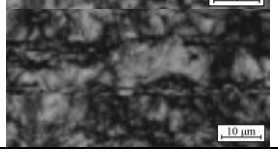	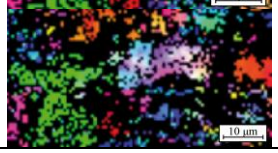	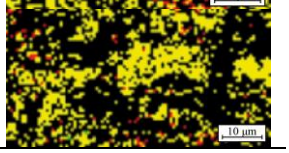

Acquisition of a high quality EBSD pattern depends on several factors, one of the most important being perfectly planar and deformation free sample surface. As it turned out during the experiments with EBSD mapping, the smoothness of sample surface presents quite a significant issue at the later stages of the deformation. Documentation of EBSD maps during the nine stops of tensile test (Figure 7) is shown in Table 2.

Reasonable quality EBSD patterns were obtained up to about 10 % elongation of the sample. Further deformation creates visible surface relief which effectively disturbs EBSD mapping of the sample. As this value emerged as a critical one for several test of this steel, it seems to be a generally applicable value of elongation up to which reliable in-situ EBSD analysis can be performed on the multiphase steel based on ferrite – carbide free bainite microstructure. This is in good agreement with other works [11, 12], which also published EBSD maps obtained at smaller deformations up to about 10% only. The IPF-Z images (inverse pole figures in the direction perpendicular to sample surface) demonstrate that during the straining relatively large grains of free ferrite get fragmented into several sub-grains with various crystallographic orientations. The orientation misfit is originally small and increases gradually with increasing applied load. The sub-grains were further fragmented down at high loads.

4 Conclusion

In-situ tensile straining of three low alloyed TRIP steels with the same chemical composition, but various annealing temperatures of 800 – 950°C was performed. The microstructures consisted of ferrite, bainite and around 10% of retained austenite.

Two kinds of flat samples had been design and their surfaces prepared to high standards to enable EBSD acquisition. Classical dog-bone shaped flat samples were used for EBSD analysis and most of the microstructure observations. Microstructure development at the fracture and fracture initialization and propagation have been observed during the staining of curved sample Thinned middle area of the sample localized fracture into this particular area, making it easier to notice fracture initiation during the testing. Cracks initiated at sample surface and propagated along ferrite-bainite interphase.

It has been further found out, that bulky ferrite grains can split into several sub-grains with different lattice orientations during the straining. Lattice misfit between the sub-grains was gradually increasing with increasing load. EBSD analysis was possible up to 10% deformation, as the number of zero solutions increased significantly at higher deformations.

5 Acknowledgement

The present contribution has been prepared under project LO1502 ‘Development of the Regional Technological Institute‘ under the auspices of the National Sustainability Programme I of the Ministry of Education of the Czech Republic aimed to support research, experimental development and innovation.

6 References

[1] Chen Q Z, Chu W Y, Wang Y B, Hsiao C M 1995 *Acta Metall. Mater.* 43 4371-6.
[2] Yuan Z Z et al. 2006 *Mater. Charact.* 56, 79-83.
[3] Chena F F, Hwang J, Yu G P, Huang H H 1999 *Thin solid Films* 352 173-8.
[4] Guo E Y et al. 2013 *Mat.Sci.Eng. A* 580 159-68.
[5] Muránsky O, Šittner P, Zrník J, Oliver E C 2008 *ActaMater*. 56 3367–79.
[6] Aišman D et al. 2008 Proc Annals of DAAAM and Proceedings of the International DAAAM Symposium Ed. B. Katalinic DAAAM International Vienna 7-8.
[7] Kučerová L, Jirková H, Mašek B 2016 *Manufacturing Technology 16* (1), 145-9.
[8] Mašek, B et al. 2007 *Mechanical Behavior of Materials X*, 1 – 2, 345-346, 943-6.
[9] Jirková H et al 2015 *Mater Today* 2S, 627-30.
[10] Pereloma E V et al. 1999 *Mat.Sci.Eng. A* 273-275, 448-52.
[11] RYU J H et al. 2010 *Scripta Mater.* 63 297–9.
[12] LI W S et al. 2016 *Mat.Sci.Eng*. A 649 417-25.